CRYSTAL GROWTH & DESIGN

pubs.acs.org/crystal

Article

Simulation of Crystal Growth by an Innovative Hybrid Density Functional Theory Continuum Solvation Approach: Kink Site Formation on Barite (001)

Stefan Rudin,* Piotr M. Kowalski, Martina Klinkenberg, Thomas Bornhake, Dirk Bosbach, and Felix Brandt

Cite This: *Cryst. Growth Des.* 2024, 24, 159−170

Read Online

ACCESS | Metrics & More | Article Recommendations | Supporting Information

ABSTRACT: We have tested the ability of a hybrid density functional theory (DFT)−continuum solvation approach to simulate processes relevant to sorption and crystal growth at the solid−water interface with the largest possible accuracy. The focus was on the study of Ba^{2+} kink-site nucleation at the (001) surface relevant for barite growth. For the first time, a complete Ba^{2+}-ion uptake process at the water mineral interface was simulated using ab initio-based methods while maintaining reasonable computational effort. The Ba^{2+} attachment path is mainly determined by dehydration of the attached ion and chemical bond formation. For all intermediate steps starting from the hydrated ion to the completely attached ion, a full representation of the chemical bonds as well as effects of the aqueous phase were considered. Previous results of simulations with classical force fields could be qualitatively reproduced, and new details on the attachment path emerged. This study indicates that energy differences between Ba^{2+} attachment processes at different sites are mainly due to the influence of step morphologies at the atomic scale. The hybrid DFT continuum solvation approach enables ab initio-based simulations of solid surface−aqueous interfaces, which may be applied to other relevant problems, for example, adsorption processes, complex formation at surfaces, or electrochemical processes.

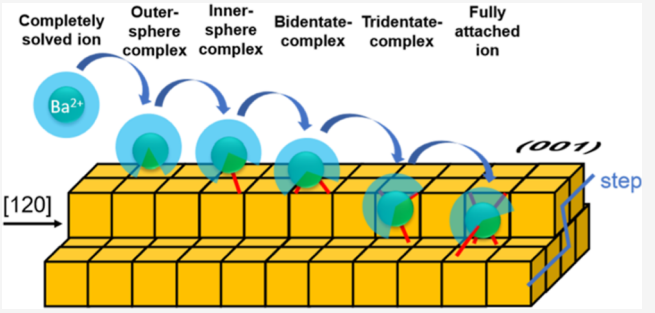

INTRODUCTION

Processes at the solid−aqueous solution interface, such as crystal growth, adsorption, and structural uptake of radionuclides in aqueous solution or complex formation, are of great relevance in numerous current topics of energy and climate research, such as nuclear waste disposal, hydraulic fracking, or electrochemistry.[1−8]

The ion attachment processes from the aqueous solution to the solid that takes place during crystal growth are usually complex multistep processes that include several intermediate steps such as the formation of outer-sphere and inner-sphere complexes.[9−12] However, the fundamental processes at the atomic scale are poorly understood. One reason for this is that sorption processes or the structural incorporation of ions into a growing crystal surface have been only incompletely simulated. Correlations of these processes with microscopic and macroscopic observations are missing even for very well studied minerals like barite and calcite.[13]

Precipitation of sparingly soluble barite from groundwater leads to scale formation. The isostructural uptake of Ra can result in technically enhanced naturally occurring radioactive material (TENORM).[4−7] The formation of solid solutions is also important for radionuclide retention in nuclear waste repositories, e.g., by incorporation of Ra into barite or of Se and Ra into the calcite structure.[14,15] Retention of Ra by cementitious phases can occur via sorption processes, such as complex formation at the solid−water interface or incorporation into the solid phase by solid solution formation.[16] Moreover, the accurate description of water adsorption on metal surfaces is of interest in current topics in electrochemistry, such as catalysis, water electrolyzers, and fuel cells.[3,8]

In the case of barite, experimental work as well as simulation studies show that the most stable surfaces are the (001) and (210), consequently determining the morphology of the barite crystal, and thus are most relevant to barite growth.[17−20] In situ atomic force microscopy revealed strongly anisotropic crystal growth of the barite (001) surface, which is controlled by the attachment of ions to ⟨120⟩-steps.[18,21,22] Barite

Received: July 7, 2023
Revised: November 20, 2023
Accepted: November 28, 2023
Published: December 15, 2023

symmetry leads to the formation of obtuse and acute ⟨120⟩-steps, with different growth rates.[23−25]

Activation energies for (001) surface growth range from 35 ± 8 to 38 ± 4 kJ/mol and were determined by macroscopical and microscopical experimental growth rates.[21,22,26] Vital et al.[26] determined the same activation energy of 35 ± 2.5 kJ/mol for (001), (210), and (101) surface growth and postulated that the reaction rate is surface-controlled with the same rate-limiting step for all of these.

For barite (001) growth, during kink-site nucleation, the first ion attachment at an ⟨120⟩ step to start a new row parallel to that step is considered to be the rate-limiting step that controls the kinetics of crystal growth. This occurs from the hydrated ion to the completely attached ion by dehydration and chemical bond formation in several steps.[9,27] From there, barite continues to grow anisotropically in both directions. Due to the symmetry of the barite, four distinctly different sites for kink nucleation exist for both the Ba^{2+} and SO_4^{2-} attachment. These are acute step, high; acute step, low; obtuse step, high; and obtuse step, low (Figure 1). In this study, we only consider Ba^{2+} attachment following studies of Stack et al.[9] However, the question whether Ba^{2+} or SO_4^{2-} kink-site nucleation is the rate-limiting is still under debate.[18,25,27,28]

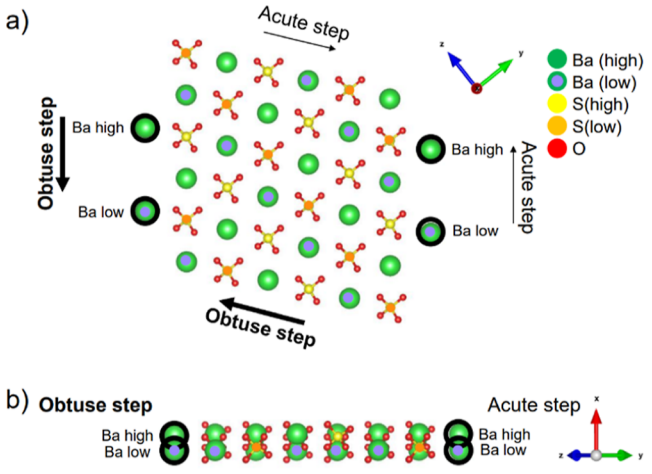

Figure 1. Ba^{2+} attachment positions on the ⟨120⟩ steps of the barite (001) surface: (a) perpendicular *x* and (b) parallel *x*. The barite structure was visualized with the VESTA software.[29]

Pina et al.[18] were able to provide energy differences of attached ions at different sites using kinetic Monte Carlo (KMC) and molecular dynamics (MD) simulations. Kink-site nucleation processes are postulated to be endothermic, whereas the further step growth processes are exothermic. SO_4^{2-} was assumed to be attached preferential due to its lower energy compared to Ba^{2+}. Water was considered only in the form of experimentally determined hydration energies, which were added to the simulation results.

Stack[27] simulated different sites of attached Ba^{2+} and SO_4^{2-} ions in an aqueous environment and concluded that the rate-limiting step was the exothermic Ba^{2+} attachment. Ba^{2+} as well as SO_4^{2-} attachment as the rate limiting process of the growth on the (001) face at the same Ba^{2+} to SO_4^{2-} ratio under close-to-equilibrium conditions, are suggested in the literature.[25,28] Crucial to the relevance of the individual attachment processes to different sites for crystal growth is their activation energies. To obtain these, complete reaction pathways of the attachment processes, including the rate-limiting steps, must be determined starting from the fully dissolved ion and including water.

Stack et al.[9] were the first to simulate a complete ion attachment/detachment process at the (001)-barite surface (kink-site nucleation) including water using classical force-field-based MD simulations, metadynamics method, and umbrella sampling, to describe the kinetics of the process. The simulations assume Ba^{2+} kink-site formation as the rate-limiting step. Their attachment path had several intermediate steps: (1) the fully solvated Ba^{2+} ion in aqueous solution, (2) the outer-sphere complex, (3) the inner-sphere complex, (4) the bidentate complex, and finally (5) the Ba^{2+} ion fully attached to the barite surface (Figure 2). The rate-limiting step is the escape from the inner spherical complex, which is also the structure with the lowest energy. The activation energies of the rate-limiting steps for attachment and detachment of 41 ± 13 and 34 ± 4 kJ/mol could be obtained by a separate simulation approach, the reactive-flux-method. Formation of inner-sphere complexes and thus the same rate-limiting step is postulated for all possible Ba^{2+} kink formation positions.

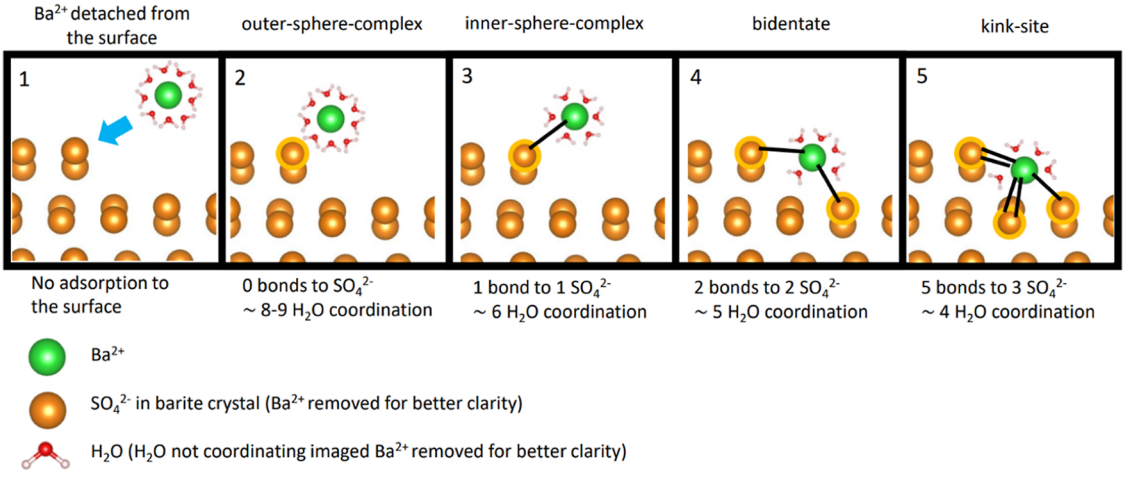

Figure 2. Minimum energy structures occurring during Ba^{2+} detachment at the ⟨120⟩ step of the barite (001) surface according to Stack et al.[9]

https://doi.org/10.1021/acs.cgd.3c00809
Cryst. Growth Des. 2024, 24, 159−170

However, a single attachment process is not able to explain the anisotropic step growth of the entire (001) surface. An ensemble of different attachment processes on the molecular scale is assumed to explain microscopically observed barite growth and hence the experimentally determined activation energies.[13,25,30,31] It is not yet known which attachment processes at which sites are relevant for the phenomenologically observed anisotropic island growth.[13,24,32] The force fields used in classical MD simulations can usually only approximate chemical bonding. A more accurate description requires an ab initio treatment, which, however, requires high computational power and thus usually focuses only on specific aspects of the processes.[33] However, a computationally efficient method that simulates complete ion attachment processes ab initio and with the inclusion of water in all steps is still missing.

The aim of this study is to test and verify a combination of methods that allows for the simulation of complete ion attachment processes, including all intermediate steps relevant for crystal growth and sorption processes at the solid−water interface with the highest possible accuracy. A mandatory prerequisite for such a method is the correct simulation of chemical bonds as well as of the water as bulk, sorbed at the solid surface, and the hydration shells of dissolved ions. At the same time, the necessary computational effort must be reasonable. Here, we test a combined density functional theory (DFT), nudged elastic band method (NEB), and soft-sphere continuous solvation (SSCS) methods. Computationally intensive ab initio DFT is used because it simulates all electrons relevant to chemical bonds explicitly, in contrast to force-field based methods. However, ab initio DFT often leads to an insufficient description of water, as van der Waals forces and hydrogen bonding are inadequately described.[34] A continuum solvation approach developed by Andreussi et al.[34] and Fisicaro et al.[35] provides a remedy. Here, water is implicitly described by a force field that depends only on its dielectric constant. This permits a correct simulation of bulk water, hydration of dissolved ions, and the mineral−aqueous solution interface. The computational effort is also drastically reduced by eliminating the explicit water molecules. NEB allows single long and complicated reaction pathways to be simulated ab initio without the use of additional methods. Unlike in the case of ab initio MD, long and complicated pathways can be simulated with reasonable computational effort, by focusing on selected processes. This combines both ab initio and continuum force field-based methods, which provide the highest possible accuracy in aspects relevant to the simulations, while maintaining a reasonable computational cost.

Here, we test the ability of DFT continuum solvation schemes to simulate the Ba^{2+} attachment process at the barite−water interface at the quantum mechanical level. We were interested in verifying the level of quality at which these methods match previous force-field based simulations and whether these schemes can improve the description of crystal growth processes at the interface. For this reason, the possibility of SO_4^{2-} kink-site nucleation is not considered here.

METHODOLOGY

Setup of DFT-Simulations. The DFT simulations were performed using the Quantum-ESPRESSO package.[36,37] We applied the PBE exchange−correlation functional,[38] as it resulted in the best match of the computed to measured lattice parameters (see Appendix: Table A1). The planewave energy cutoff of 50 Ry was applied, and the core electrons of the system were replaced with ultrasoft pseudopotentials.[39] The hydration effects have been simulated with the SSCS scheme.[35] In this approach, the system is split into two subsystems: the barite crystal computed at the DFT level and the aqueous phase simulated as a continuum medium characterized by its dielectric constant, $\varepsilon = 78.4$.[34,35,40−42] The calculations were performed with the Environ simulation package.[34,35,37,40] Detailed information on the SSCS-method is provided in refs 34 and 35.

In the SSCS approach, each atom is assigned a radius that defines the solvation sphere, within which the solvent is excluded. The default radii of the solvation spheres are taken as the universal force field (UFF) values.[43] These for the considered species are reported in Table 1.

Table 1. Default UFF Values[43] Used for Solvation Radii in SSCS

element	default UFF-values [Å]
Ba	3.703
O	3.500
S	4.035

A continuous switching function ensures a smooth transition of the permittivity constant at the solvation sphere boundary, from the vacuum value of $\varepsilon = 1$ to that of the bulk solvent.[35] The rescaling of the solvation sphere radii (cavity multiplying factor) is often practiced reproducing some experimental data, including solvation enthalpies. For instance, UFF radii require a scaling factor of 1.13 to reproduce free energies of hydration of a large set of solvated cations.[35] This shows that a direct comparison between the applied and measured sizes of the ionic species should be avoided. The reason is that the ionic radius used in the calculations strongly depends on the softness parameter regulating the transition behavior of the switching function. The applied ionic radius can easily vary by more than 1 Å between identical solutions considering different values of the softness parameter.[35]

The energy path describing the attachment process was simulated with the NEB as implemented in the Quantum-ESPRESSO package.[36,37,44−46] The Climbing Image method (Cl-NEB) was used to ensure that the highest transition state is reached.[45] Due to the complexity of the pathway, the calculations were divided into two paths, assuming the intermediate state of a minimum energy configuration as end structure for the first and starting structure for the second pathways. The two pathways were computed with 20 and 30 images, respectively.

Construction of the Barite Surfaces. The nine barite surfaces [(001), (210), (010), (100), (011), (101), (012), (201), and (211)] relevant for barite crystal growth[20] were created for computing their surface energies [e.g., (001) and (210) see Figure 3a,b]. The barite structures in the figures were visualized with the VESTA software.[29] All structures computed in this study are available in the data publication (ref 47). Each of the surfaces was described by multiple layers of $BaSO_4$, referred to as slab. These consisted of five or six barium layers, depending on the target symmetry of the system (see Appendix: Figure A1). To avoid interactions between the repeating slabs along their surface normal, a distance of 10 Å perpendicular to the slabs was applied.[48] The top and bottom

https://doi.org/10.1021/acs.cgd.3c00809
Cryst. Growth Des. 2024, 24, 159−170

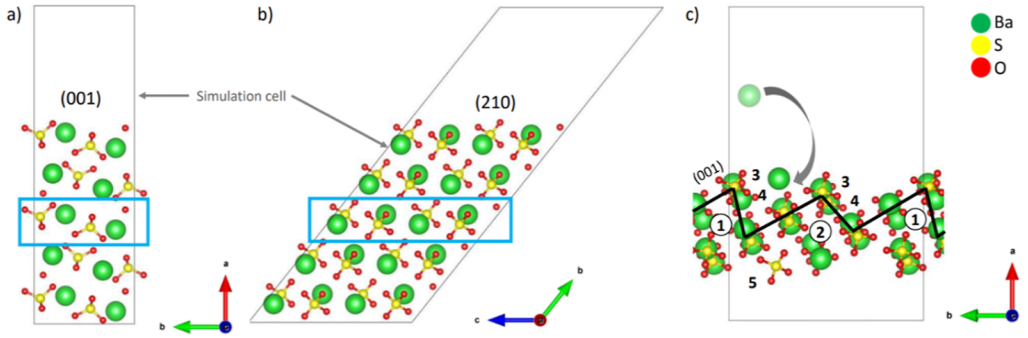

Figure 3. (a) Barite (001) and (b) (210) slab cells. The blue squares indicate fixed atoms; all other atoms are set free to relax. (c) Slab cell of the barite (001) surface (black line) including the acute (1) and obtuse ⟨120⟩ steps (2), both with high (3) and low positions (4). A dissolved Ba^{2+} ion was attached to the low position (4) of the acute ⟨120⟩ steps (1). Additional SO_4^{2-} was added at the bottom of the slab to keep the system in charge balance (5).

Table 2. Barite Surface Formation Energies (in J/m^2) Calculated for Surfaces in a Vacuum and for Hydrated Surfaces[a]

barite surfaces	rank: surface energies	this study (vacuum)	DFT[20]	MD[17]	MD[19]	this study (hydrated)	exp[50]
(210)	1	0.27	0.37	0.42	0.52	0.038	
(001)	2	0.29	0.38	0.40	0.62	0.022	0.025
(101)	3	0.38	0.53	0.51		0.064	
(211)	4	0.40	0.46	0.55		0.050	
(010)	5	0.41	0.55	0.61	0.73	0.069	
(011)	6	0.43	0.60	0.66		0.074	
(100)	7	0.50	0.64	0.66	0.89	0.144	
(012)	8	0.55	0.82			0.138	
(201)	9	0.62	0.64			0.043	

[a]Results of previous computational DFT and MD studies for the cases of the surface in vacuum are also provided. The value measured by ref 50 for the hydrated (001) surface is given in the last column.

layers of the slab were relaxed. The atom positions in the center of the slabs were fixed, retaining the bulk crystal structure.[49]

For the simulation of crystal growth on the barite—(001) surface—a stepped surface slab with a thickness of two barite unit cells was constructed (Figure 3c). It includes the ⟨120⟩ obtuse and acute steps and provides all four sites for both Ba^{2+}- and SO_4^{2-} attachment relevant for barite (001) surface growth.

The upper half of the slab was relaxed, whereas the lower section was fixed and considered bulk barite. The optimized parameters for bulk barite were also applied for the stepped surface calculations. The stepped (001) surface was tilted toward the *y*-direction. This avoids additional steps and other surface effects, while maintaining the periodicity of the slab in all three dimensions. A vacuum layer of about 15 Å was added between the slabs to leave enough space for simulating the attachment process and to minimize unwanted interactions.

The setup of the (001) surface with ⟨120⟩ steps was used as basis for simulating Ba^{2+} kink-site nucleation. In order to simulate the complete attachment process, two structures were created, representing the initial state, referred to as the start structure, and the end of the Ba^{2+} ion attachment process, referred to as the end structure, respectively. For the starting structure, the attaching Ba^{2+} ion was fixed in a position in the middle of the aqueous phase between the periodically repeated slabs. For the end structure, the attaching Ba^{2+} ion was placed at the appropriate site at the ⟨120⟩ step on the slab, and all atomic positions of the system were relaxed to the equilibrium position. To preserve charge neutrality, a SO_4^{2-} ion was placed as a counterpart on the other side of the slab as far as possible from the postulated attachment pathway for Ba^{2+} kink-site nucleation. Test simulations with larger four Ba-layer slabs gave very similar results, indicating the absence of any artificial effects associated with this placement of ions.

RESULTS AND DISCUSSION

Barite Bulk Phase and Its Termination. In order to understand the stability of different surface facets, we constructed models of nine barite surfaces, using studies of Bittarello et al.[20] as a guidance. The surface energies of all the models were computed and results compared to prior knowledge.[17,19,20,33] The obtained surface energies and their relative order are comparable to values reported in the literature.[17,19,20] Consistently, all studies show that the (001) and (210) surfaces are the most stable (Table 2).

Simulation of Aqueous Solution. Hydration energy of aqueous ions is often used to check the quality of the applied computational method. This was done in studies of Stack and Rustad[51] and Stack.[27] In the frame of the applied DFT-SSCS computational scheme, it is a common practice to rescale the sizes of the cations to match, for instance, the hydration enthalpy. This is done with selecting an ion radius scaling parameter α. The results in Table 3 show that the calculation of the first hydration shell of the Ba^{2+} ion with an alpha-value of 1.13 delivers the most realistic values for hydration energies compared to literature values.[52,53] However, applying such a setup to the calculation of barite surface results in physically unreasonable results, for instance, the hydrated (001) surface being unstable (Figure 4).

We therefore used α-values of 1.255 and 1.270. The first value matches the difference between the start and end structure of about 21 kJ/mol determined by simulations of

https://doi.org/10.1021/acs.cgd.3c00809
Cryst. Growth Des. 2024, 24, 159−170

Table 3. Hydration Energies of Ba^{2+} as a Function of Scaling Parameter α

DFT-SSCS (this study)	scaling parameter α	$20 \times 20 \times 20$ Å^3 cell $\Delta H_{hydration}$ [kJ/mol]	slab cell[a] $\Delta H_{hydration}$ [kJ/mol]
	1	−1892	−1885
	1.05	−1610	−1603
	1.1	−1418	−1412
	1.12	−1357	−1351
	1.13	−1329	−1323
	1.15	−1278	−1272
	1.2	−1168	−1162
	1.25	−1078	−1073
	1.27	−1046	−1041
	1.3	−1002	−997
reference		method	$\Delta H_{hydration}$ [kJ/mol]
Persson et al. 1995,[52] Richens 1997[53]		calorimetry	−1305
Marcus 1991[54]		thermodynamic calculations	−1210
Smith 1977[55]		thermodynamic calculations	−1320
			−1270
Stack 2009[27]		MD	−1301

[a]According to Figure 1c.

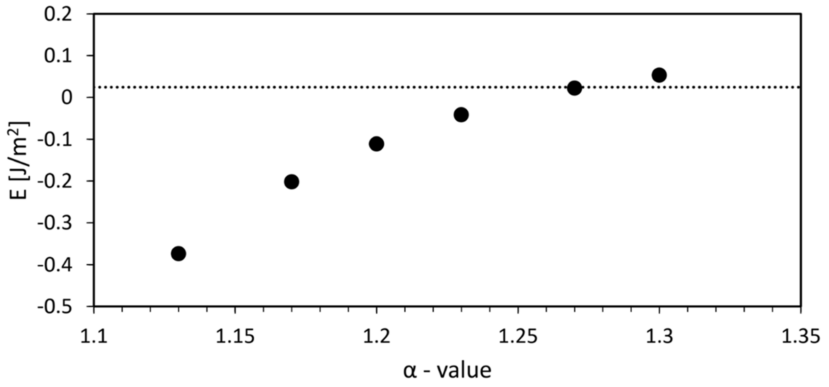

Figure 4. Formation energies of the hydrated barite (001) surface, obtained with the DFT-SSCS scheme, applying different α parameter values. The dashed line indicates the experimental value.[50]

Stack et al.[9] With an α-value of 1.270, the end structure is energetically favored by an energy difference of 31 kJ/mol compared to that of the start structure. This fits with the results of Stack et al.,[9] who determined this value between the minimum energy structure with the highest and lowest energy.[9] However, increasing the α-value from 1.130 to 1.255 or 1.270 leads to an underestimation of the hydration energies of the Ba^{2+} ion (see Table 3). On the other hand, the hydrated barite (001) surface formation energy of 22 mJ/m^2 computed with the α value of 1.27 matches well the measured value of 25 mJ/m.[2,50] As shown in Figure 4, such a good fit could be obtained only with the α value around 1.27, and for smaller values, e.g., 1.13, the surface formation energy becomes unrealistically large and negative, making the (001) surface unstable.

Surface Relaxation in the Presence of Aqueous Phase. Being the most stable, the (001) and the (210) barite surfaces are most relevant for barite growth. We thus performed simulations of the relevant barite−aqueous phase interfaces. Figure 5a−c,d−f shows the results, respectively.

Figure 5 shows the resulting polarization density of the solvent, resembling a physical boundary between the solvent and the interface. The difference in interfacial polarization is caused by different local charge of the Ba^{2+} and SO_4^{2-} ions at the surface.[34,35] The calculations of the hydrated surface show vertical displacements that are smaller than the respective displacements of surface atoms relaxed under vacuum conditions (see Appendix: Figure A2). Consequently, the positions of surface atoms of both considered surfaces in contact with water are more similar to those of bulk barite. This is consistent with experimental findings showing that the structure of the interface is a continuation of the bulk barite crystal structure.[56,57] However, small differences are apparent. The SO_4^{2-} groups in the topmost layers are more distorted, comparing the position of the sulfur ion to the Ba^{2+} ions and slightly rotated compared to bulk barite. This is consistent with experimental observations.[56,57] In the case of the (001) surface, there are discrepancies in both displacement amplitudes and directions along the surface normal, already noticed in the literature itself.[56,57] According to Bracco et al.,[57] these differences arose due to different levels of accuracy and difference in approach and number of measurements. Differences between the MD simulations and experiments were explained by the presence of solvated Ba^{2+} and SO_4^{2-} ions under experimental conditions and continuous adsorption of these species to the barite surface, which influences the barite interface atom relaxations.[57] We note that this effect is not accounted for in our study.

https://doi.org/10.1021/acs.cgd.3c00809
Cryst. Growth Des. 2024, 24, 159−170

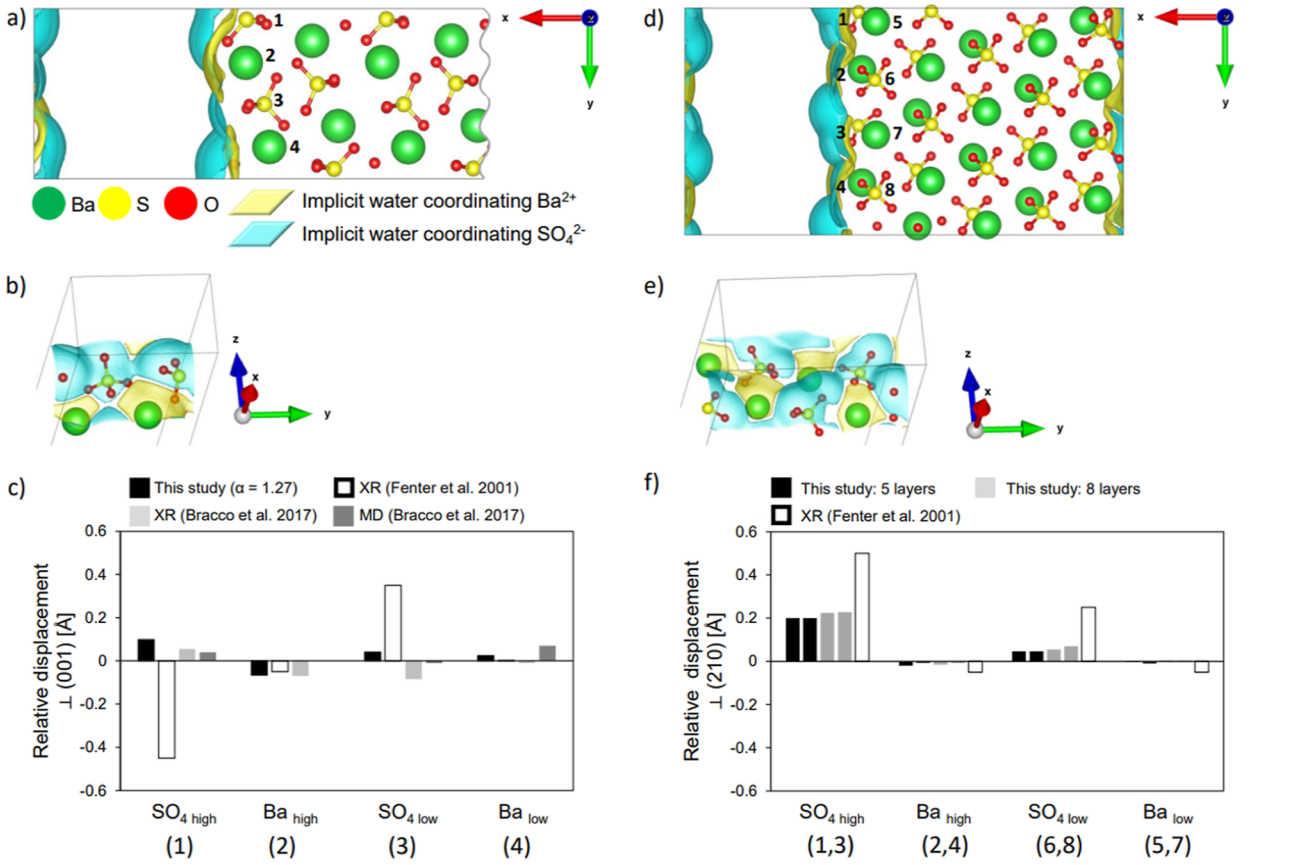

Figure 5. (a) Simulation cell of the barite (001) water interface. The adsorbed implicit water is colored yellow and blue. Bulk water is not indicated in the pictures for clarity. The Ba^{2+} and SO_4^{2-} ions in the topmost interface layer are highlighted (1−4). (b) 3D Image of the barite−water interface layer from (a). (c) Vertical displacements of the barite (001) atoms (1−4) compared to literature values.[56,57] (d) Simulation of the barite (210) water interface. The adsorbed implicit water is indicated in yellow and blue. Bulk water is not indicated in the pictures for clarity. The Ba^{2+} and SO_4^{2-} ions in high positions (1−4) and low positions (5−8) of the topmost interface layer are highlighted. (e) 3D Image of the barite−water interface layer from (d). (f) Vertical displacements of the barite (210) atoms (1−8) with respect to bulk barite compared to Fenter et al.[56]

The simulations of the (210) surface with a slab consisting of five layers show that the Ba^{2+} distortions along the surface normal are slightly oriented into the crystal. Using a surface slab consisting of eight Ba layers and relaxing three of them on each side, the same shift occurs (see Figure 5f). This is consistent with experimental values.[56] We note, however, that in both cases, the relaxations are marginal and within the range of the errors. The obtained distortion of the SO_4^{2-} ions is significantly lower compared to the literature values, but also with consistent direction of the distortion. Since no significant differences in vertical distortion of the SO_4^{2-} ions have been observed in calculations with the five- and eight-layer slab, limitation of the model due to the low number of relaxed barite layers can be excluded.

Ba^{2+} Attachment. Figure 6 shows the simulated energy pathway for the attachment of one Ba^{2+} ion to the acute ⟨120⟩-step of the (001) surface in aqueous solution. We selected the Ba_{low} attachment site exactly the same as in the study of Stack et al.[9] This was done to directly compare the performance of the DFT-NEB-SSCS method to the results of the classical force field-based approach. However, the Ba_{low} position occurs at both the obtuse and acute ⟨120⟩ steps of the (001) surface.[58] We note that the Ba^{2+} attachment simulations of Stack et al.[9] was performed at the acute step, which is also the case we study. According to the KMC simulations, this step is considered to be the slower growing of the two ⟨120⟩ steps.[24,32] In general, the attachment of the first ion forming a new kink site is considered to be the step with the highest activation energy compared to further attachment of ions continuing the row.[9,18,27] On the other hand, the computed attachment path could also represent detachment of a Ba^{2+} ion from the ⟨120⟩ step.[9,33,46] However, the rate-limiting step for dissolution is considered to be the removal of the first ion from an already existing row.[27] In view of these discrepancies, the pathway considered and computed here for Ba^{2+} attachment/detachment should not be considered the rate-limiting process for barite (001) dissolution and possibly not for (001) surface growth. The purpose of this work is to compute the pathways already considered in the studies with classical force fields to assess the performance of the DFT-SSCS method.

In the considered pathway, the attachment process starts with the completely solved Ba^{2+} ion in aqueous solution (Figure 6a) (1). During the approach of the Ba^{2+} ion to the stepped barite surface, the formation of the outer-sphere complex represents the first local minimum of the pathway (2,3). After overcoming an energy barrier, an inner-sphere complex forms, resulting in the second energy minimum (4). This is characterized by forming one chemical bond from the attaching Ba^{2+} ion to the barite surface.[9] The Ba^{2+} attachment path reveals two additional, local energy minima, both representing inner-sphere complexes (5, 6). The energy barrier between the two inner-sphere complexes results from rotation

https://doi.org/10.1021/acs.cgd.3c00809
Cryst. Growth Des. 2024, 24, 159−170

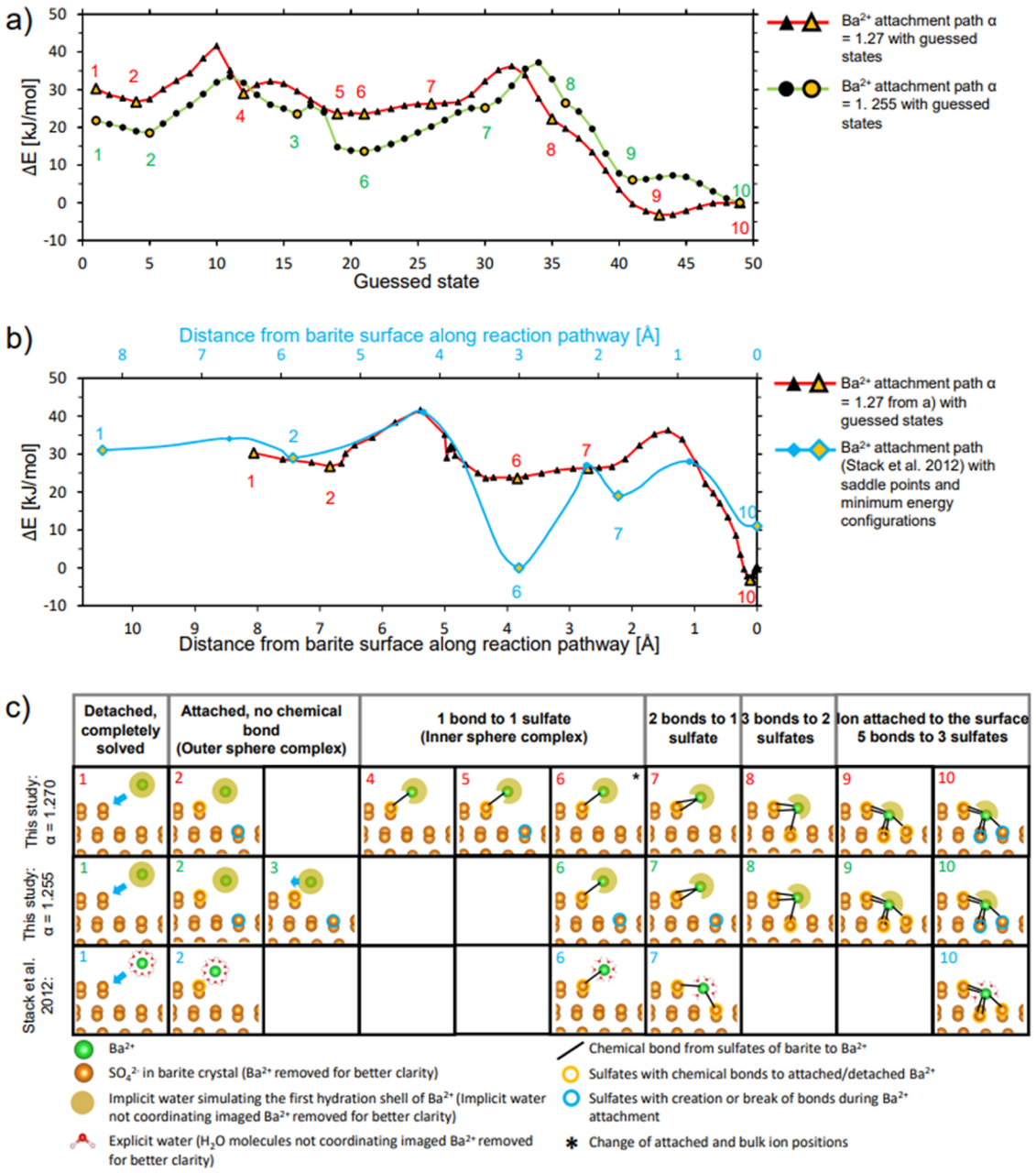

Figure 6. (a) Ba^{2+} attachment/detachment path with an α-value of 1.270 and 1.255 derived from DFT-NEB-SSCS calculations. The distance end energy of the completely attached ion is set to 0 in both cases. (b) Comparison of the Ba^{2+} attachment/detachment path of this study (α = 1.27) performed with DFT−NEB-SSCS (red) with the path of Stack et al.[9] (blue). Note the different scales of the *x*-axes for both attachment/detachment paths. The energy paths are plotted so that the distance (along the *x*-axis) of the highest saddle points of both lines match. (c) Illustration and comparison of the highlighted guessed states in (a,b) of the attachment/detachment paths for Ba^{2+} from this study with Stack et al.[9]

of one SO_4^{2-} and a change of its chemical bonding to Ba^{2+}-ions. The transition to the energy minimum of the third inner-sphere complex is associated with further relaxations of the barite inner structure of the barite slab. According to Stack et al.,[9] a further approach of the Ba^{2+} ion to the barite surface results in the formation of a bidentate complex, in which the Ba^{2+} ion has two chemical bonds to two oxygen atoms of the same SO_4^{2-} ion at the high position of the step (7). However, in our simulations with the DFT-SSCS method, this configuration is not stabilized. The completely attached Ba^{2+} ion forms five bonds to three SO_4^{2-} (9, 10).

In summary, the considered reaction pathway can be divided into two parts, separated with an inner-sphere complex as an intermediate state. The resulting energy barriers among the three configurations determine the activation barriers for the attachment/detachment processes. This is also the reason for dividing our simulations into two separate subpaths. Figure 6b shows the comparison of the pathway derived with the DFT-NEB-SSCS approach with the path derived by Stack et al.[9] Both pathways show similar features (Figure 6b). These are the bidentate structure, the inner-sphere and outer-sphere complex.[9] Overall, the DFT-SSCS results are qualitatively consistent with the classical force-field simulations of Stack et al.[9] The energy pathway obtained here differs only slightly in both the number of local energy minima and energies.

https://doi.org/10.1021/acs.cgd.3c00809
Cryst. Growth Des. 2024, 24, 159−170

Activation Energies and Rate-Limiting Steps. Using an α-value of 1.27, two of the simulated Ba^{2+} attachment steps have similar activation energies: (1) the formation of the inner-sphere complex with an activation energy of 15 kJ/mol and (2) the transition from the inner-sphere complex to the completely attached Ba^{2+}-ion with an activation energy of 13 kJ/mol. For an α-value of 1.255, we obtained (1) 15 and (2) 24 kJ/mol. The first activation barrier is well consistent with the result of Stack et al.[9] in both cases, who obtained a value of 12 kJ/mol. Using an α-value of 1.270, the second activation energy is lower than the value of 27 kJ/mol derived in those studies, as the rate-limiting step. However, upon application of an α-value of 1.255, the results are quite consistent. Considering the detachment process, an α-value of 1.27 resulted in 41 and 15 kJ/mol for the transition to the inner-spherical complex and the final detachment, respectively. For an α-value of 1.255, we obtained 37 and 20 kJ/mol, respectively. Stack et al.[9] obtained 41 kJ/mol as the transition from inner sphere to complete detachment as a rate-determining step. We notice that these discrepancies come from significantly lower energy of the inner-sphere complex simulated by Stack et al.[9] In those simulations, this state is even more stable than the configuration with a fully attached Ba^{2+}-ion.

Experiments show activation energies for barite (001) growth processes in the range between 35 ± 2.5 and 38 ± 4 kJ/mol. These values are derived by phenomenological observations with the aid of Arrhenius plots.[21,22,26,59] These activation energies can be interpreted as the rate-limiting step of the overall surface growth. However, different activation energies are expected to contribute to the anisotropic growth of the barite (001) surface, and it is unlikely to describe it by a single attachment process.[18,27] Stack et al.[9] applied the reactive flux method to the rate-limiting steps for Ba^{2+} attachment and detachment previously determined by metadynamics and umbrella sampling. They compared the activation energies for attachment and detachment derived in this way with experimental literature values, with both matching well with the measured values. We note, however, that this match could be obtained by chance. This is because the rate-limiting step for the detachment process is not supposed to be the detachment of one ion from a positive kink site, but the ion detachment process which creates a negative kink site.[27] The detachment of the Ba^{2+} ion from a positive kink site should thus not be representative for barite dissolution.[18,27]

Since the rate-limiting step for attachment is kink-site nucleation and only the formation of one kink site is necessary to start the step growth, the one with the lowest activation energy is the rate-limiting step. Thus, positive kink-site nucleation must be at least 40 kJ/mol in all possible cases. Since the rate-limiting step of the dissolution is postulated to be the formation of a negative kink site, the detachment of a Ba^{2+} ion forming a positive kink site must be below 34 kJ/mol. Therefore, it can be assumed that the attachment process to form a positive kink site is endothermic, which is also consistent with the simulations of Pina et al.[18] This assumption is also supported by the fact that a decrease in the alpha value from 1.270 to 1.255 results in a lower energy difference between the start and end structure. A further approach of the α-values, which are closer to experimental hydration energies for Ba^{2+} (see Table 3), could result in a higher energy of the start-structure compared to the end structure. The kink-site nucleation could be a necessary step, which must occur in order to further enable crystal growth or dissolution. Due to the endothermic character of such configurations, they have the highest activation energy for Ba^{2+} attachment process and are therefore the rate-limiting step in ⟨120⟩ step growth at the (001) surface.

Influence of the Initial Position of Ba^{2+} on the Attachment Path. The investigation of the influence of the initial location of the completely solved Ba^{2+} ion on the attachment process was done by computing routs from the aqueous Ba^{2+} ion to the inner-sphere complex (Figure 7). In one of the examples, the initial Ba^{2+} ion position was moved closer to the obtuse step (Figure 7b), making the pathway more consistent to the attachment/detachment pathway of Stack et al.[9] In this scenario, the Ba^{2+} ion is forced to attach to the obtuse step. This exercise demonstrates that the initial location of the Ba^{2+} ion relative to the barite stepped surface determines to which step a Ba^{2+} ion is attached first and finally incorporated. The starting structure in Figure 7a can thus be considered as a correct initial guess for Ba^{2+} ion attachment to the acute low position on the (001) surface with ⟨120⟩ steps.

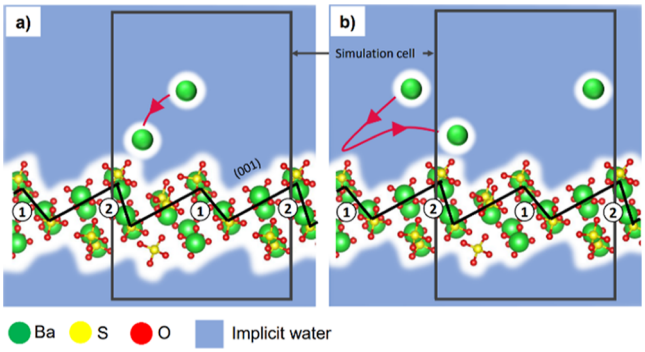

Figure 7. Start structures for Ba^{2+} attachment. (a) Attachment from the front side to the acute ⟨120⟩ step and (b) attachment from the back side to the acute step. Obtuse (1) and acute (2) steps are highlighted. The resulting attachment paths are indicated in red. Note that the simulation cell is repeated an infinite number of times in all three dimensions. The attachment path in (b) crosses the boundary of the simulation cell.

Once the inner-sphere complex is formed, one chemical bond has already been formed with respect to the barite surface. In such a configuration, diffusion seems to be unlikely during the attachment process from the inner-sphere complex to the fully attached ion.[57] This is because chemical bonds have to be broken and new bonds must be created for diffusion to happen. Such a process requires high activation energies (see Ba^{2+} attachment paths in Figure 6). Consequently, during crystal growth, the location of the first fully dissolved Ba^{2+} ion has only a significant effect on the position of attachment, until an inner-sphere complex is formed.

The Inner-Sphere Complex. Our results as well as previous studies of Stack et al.[9] show that the inner-sphere complexes play an important role as an intermediate state in the Ba^{2+} attachment/detachment process. However, the energy obtained for the inner-sphere complex differs from the result of Stack et al.[9] The reason may be a different treatment of the interatomic interactions by both studies, surface structuring of water molecules not captured by the DFT-SSCS method, or more accurate quantum mechanical approach we used. Although it is difficult to judge which method is more correct for this complex, our result may be more realistic, as the reaction pathway computed by Stack et al.[9] results in the inner-

https://doi.org/10.1021/acs.cgd.3c00809
Cryst. Growth Des. 2024, 24, 159−170

sphere complex being more stable than the fully attached ion configuration.

The four inner-sphere complexes possibly relevant for the Ba^{2+} kink-site nucleation to all four positions at the ⟨120⟩ steps of the (001) face (see Figure 1) were computed to further elucidate the energy discrepancies of the inner-sphere complexes between the attachment pathway of this study with that of Stack et al.[9] The initial structures for these studies were selected according to the configuration with the lowest energy, labeled no. 6 in Figure 6.

The Ba^{2+} ions of the inner-sphere complex of the four structures considered were set free to relax in all three dimensions. This resulted in a stable configuration in all cases. It ensures that in each case, the respective inner-sphere complex is a minimum energy structure. We note that all these structures can in principle occur during the attachment/detachment of one Ba^{2+} ion to the corresponding site. Moreover, the DFT-SSCS calculations show that all of these inner-sphere complexes have rather similar energies (see Table 4 and Figure 8).

Table 4. Comparison of Energy Differences of the Inner-Sphere Complex Located at Four Different Positions at the ⟨120⟩ Steps of the (001) Surface

Ba^{2+} attachment sites	ΔE [kJ/mol]
obtuse-high ↔ acute-high	3.74
obtuse-high ↔ acute-low	0.80
obtuse-low ↔ acute-high	0.80
obtuse-low ↔ acute-low	3.72
obtuse-high ↔ obtuse-low	4.54
acute-high ↔ acute-low	2.91

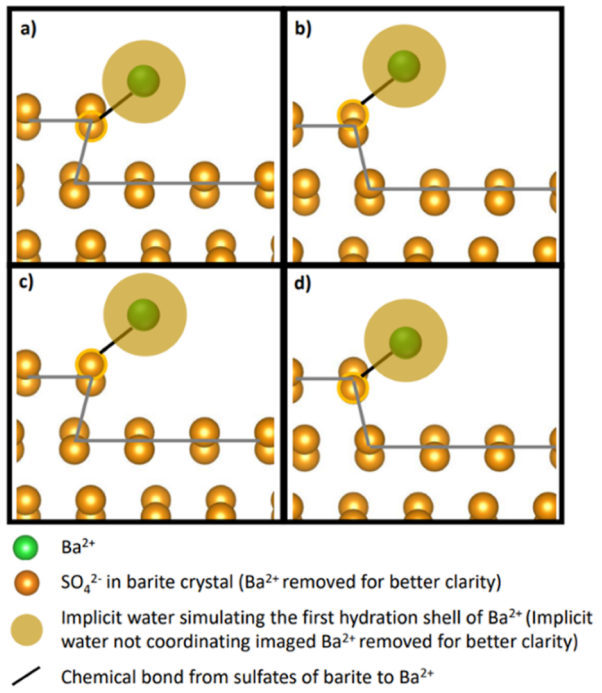

Figure 8. Simulated inner-sphere complexes of Ba^{2+} attachment to all available positions on the ⟨120⟩-steps of the (001) surface. (a) Acute step high position, (b) obtuse step high position, (c) acute step low position, and (d) obtuse step low position. The obtuse and acute ⟨120⟩ steps are indicated with a gray line.

Small differences in hydration energies of the inner-sphere complexes are unlikely to be explained by differences in coordination number of attached Ba^{2+}-ion.[52,53] Since all inner-sphere complexes are located far beyond the ⟨120⟩ steps, steric hindrance is not supposed to influence the hydration shell of these configurations. The Ba^{2+} ion within the inner-sphere complex can be assumed to have equal water coordination due to the same ion charge and size. Inner-sphere complexes of the acute-low and obtuse-high positions have similar energies. The same appears for the obtuse-low and acute-high complexes. This happens because the first two inner-sphere complexes are connected to one SO_4 in the high section of the barite ⟨120⟩ step and the other two to one SO_4 in low section of the step. As a result, the energies of inner-sphere complexes are similar and not influenced by the obtuse or acute steps. It is affected only by the position of the sulfate, where the Ba^{2+} ion is attached to.

Since the ⟨120⟩ steps do not affect the inner-sphere complexes, we can assume that this is also true for the further steps until complete dissolution. This implies that the escape of Ba^{2+} from the inner-sphere complex to the outer-sphere complex, as the rate-limiting process cannot lead to anisotropic barite (001) dissolution. The rate-limiting processes for Ba^{2+} kink-site nucleation during crystal growth in this study as well as in Stack et al.[9] are determined between the inner-sphere complex and the fully attached ion. This part of the attachment pathway is likely to be influenced by the different step and site morphologies. It may explain the anisotropic barite (001) growth as is the case with other minerals such as calcite.[60] Thus, the identified rate-limiting steps for both dissolution and crystal growth as derived here are plausible.

Bidentate Structure. The intermediate step which configuration differs the most between our study and those of Stack[27] is the bidentate complex. There is no associated minimum seen in our calculations, indicating a thermodynamical instability of this configuration.[33,46] The Ba^{2+}-ion—bidentate configuration in this study forms two chemical bonds to one sulfate. This is different compared to Stack et al.,[9] in which the Ba^{2+} is connected to two different sulfates (compare steps 7 in Figure 6). We could not stabilize a bidentate structure equal to Stack et al.[9] with the DFT + SSCS approach (Figure 9a,b). The reason is there is no water between the Ba^{2+} ion and the surface in our simulations, which leads to the attachment of the attaching/detaching Ba^{2+} ion or the formation of an inner-sphere complex.

We note, however, that this discrepancy may result from treatment of water as a continuous medium and specific selection of the SSCS parameters. Increasing the solvent filling threshold value, one of the parameters in the SSCS scheme, from 8.25D-01 to 9.50D-01, results in water intrusion in this area, leading to a stabilization of the bidentate structure (Figure 9c). The bidentate structure corresponding to Stack et al.[9] can also be simulated by computing the first hydrate shell of the attaching Ba^{2+} ion with explicit water. In this case, an explicit water molecule located in the vacuum gap stabilizes the configuration (Figure 9d).

Influence of the ⟨120⟩-Steps on Barite (001)-Face Growth. The energetical feasibility of the complete, single Ba^{2+} ion uptake allows considering this process as the main force to promote crystallization.[18,27] Therefore, the fully attached ion configuration or a possible bidentate structure could be a key to explaining the huge differences in attachment/detachment behavior at the obtuse/acute ⟨120⟩

https://doi.org/10.1021/acs.cgd.3c00809
Cryst. Growth Des. 2024, 24, 159−170

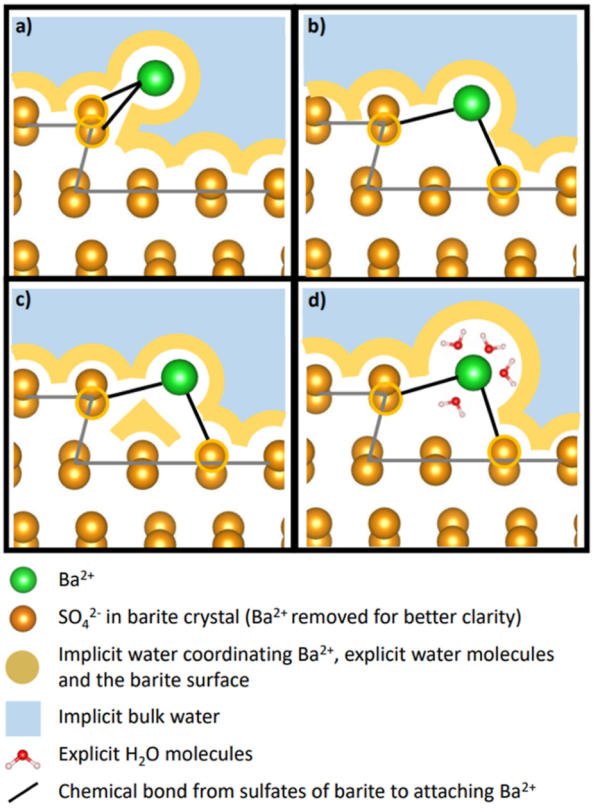

Figure 9. Bidentate complexes were calculated with DFT-SSCS. (a) Bidentate from DFT-NEB-SSCS of this study, (b) configuration according to Stack et al.,[9] (c) with increased filling threshold, and (d) with DFT-SSCS + explicit H_2O. Note the vacuum cavity in (b) between the attaching Ba^{2+} and the barite surface.

steps of the (001) face. According to Stack,[27] there are large differences in the high and low positions of fully attached Ba^{2+} ions, in both configuration and energies. There are three and five bonds for Ba_{high} and Ba_{low}, respectively. The latter was also obtained in our study. According to Stack,[27] both cases have the same water coordination ([4]). Thus, Ba_{high} is much more undersaturated, having the [12] coordination in bulk barite.[27] The fully attached Ba^{2+} ion configurations at different positions of the ⟨120⟩ steps could therefore be most likely considered as the most versatile ones. As a result, the process which is the rate-limiting step for both Ba^{2+} ion attachment or detachment scenario can be assumed to involve the fully attached Ba^{2+} ion configuration. In the energy path derived in this study, this is the case for detachment and also for the attachment process along with the formation of the inner-sphere complex. The rate-limiting step of the Ba^{2+} ion attachment process may also be the escape from the inner-sphere complex, for the case that a bidentate structure is stable. The prerequisite is that these structures also have significantly different energies at each site, Figure 6.

CONCLUSIONS

The aim of the study was to test the performance of the hybrid DFT continuum solvation approach for simulations of ion attachment processes at the solid/water interface, including the ability of the method to capture all intermediate steps relevant for crystal growth and sorption processes. For the first time, a complete Ba^{2+} kink-site nucleation process to the barite surface process was simulated using the DFT-SSCS method. The novelty is that all steps of the Ba^{2+} attachment path from the completely dissolved to the completely attached ion were described with ab initio-based methods accounting for the effect of the water solvent. In our test simulations, not only could the known results regarding barite growth from the literature be verified with this method, but also new insights could be gained.

Our simulations show that the attachment of Ba^{2+} to the ⟨120⟩ step of the (001) surface is a complicated multistep process involving several dehydration steps and the formation of outer-sphere, inner-sphere, and bidentate complexes with the barite surface. Two mechanisms mainly determine the shape of the energy pathway: bond formation and dehydration of the attached ion. The calculated Ba^{2+} attachment/detachment reaction path also sheds light on the interfacial ion diffusion phenomena during crystal growth.

Simulations compared with the classical force-field based approach of Stack et al.[9] show the same intermediate states, but with different energies. These simulations also show more details, such as additional lower energy minima, which have not been described in the earlier literature. These are caused by relaxation, the formation and break of chemical bonds, restructuring of ions, and rotations of the sulfate ions in the barite caused by addition of the Ba^{2+} ion. Inner-sphere complexes were shown to be possibly stable configurations upon Ba^{2+} ion attachment for kink-site nucleation at all four sites at the ⟨120⟩ steps of the (001) surface. Although these have similar energies, simulations using the DFT-NEB-SSCS method show small differences that are determined solely by chemical bonding to the sulfate to which they are attached. It challenges the assumption of Stack et al.[9] that the escape of a Ba^{2+} ion from the inner-sphere complex at these sites is the rate-limiting step for barite (001) dissolution. This study supports the idea that energy differences between ion attachment processes at different sites on the barite (001) face are mainly due to the influence of the different ⟨120⟩ step morphologies. This was also reported for other mineral surfaces, e.g., calcite and dolomite (104) faces.[11,60,61]

The simulations with the DFT-NEB-SSCS method show the capability of the method to simulate solid aqueous interfaces, which can be explored and applied to other relevant areas of energy and climate research such as nuclear waste disposal or electrochemistry. Even long and complicated ion incorporation processes can be simulated ab initio, while maintaining reasonable computation time. Complete surface processes at the solid−liquid interface can be simulated with good accuracy, allowing for a comparison between different sites. Unresolved complex questions, concerning not only complex formation during sorption processes on, e.g., clay minerals considered for immobilization of radionuclides but also complicated multistep processes relevant for solid solution formation, e.g., in carbonates or sulfates, can be addressed. For example, complete incorporation processes of foreign ions such as ^{79}Se into the calcite or Ra into the barite structure relevant for radionuclide retention in repositories can be simulated. Accounting for hydration of solid surfaces offers another potential application of this method such as simulating processes that occur in confined spaces like pores, e.g., nucleation, crystal growth, and dissolution. Results from simulations of the DFT-NEB-SSCS method can also be used in other simulations such as KMC to close the gap between processes on the atomic scale and phenomenological observations.

https://doi.org/10.1021/acs.cgd.3c00809
Cryst. Growth Des. 2024, 24, 159−170

■ ASSOCIATED CONTENT

Supporting Information

The Supporting Information is available free of charge at https://pubs.acs.org/doi/10.1021/acs.cgd.3c00809.

Slab structures and vertical displacements (PDF)

All structures calculated in this study are available in the data publication: 10.26165/JUELICH-DATA/7H8VDF

■ AUTHOR INFORMATION

Corresponding Author

Stefan Rudin − *Institute of Energy and Climate Research (IEK-6)—Nuclear Waste Management, Forschungszentrum Jülich GmbH, 52425 Jülich, Germany;* orcid.org/0000-0002-4857-7322; Phone: +49 2461 61 6702; Email: s.rudin@fz-juelich.de

Authors

Piotr M. Kowalski − *Institute of Energy and Climate Research (IEK-13)—Theory and Computation of Energy Materials, Forschungszentrum Jülich GmbH, 52425 Jülich, Germany; Jülich Aachen Research Alliance JARA Energy & Center for Simulation and Data Science (CSD), 52425 Jülich, Germany;* orcid.org/0000-0001-6604-3458

Martina Klinkenberg − *Institute of Energy and Climate Research (IEK-6)—Nuclear Waste Management, Forschungszentrum Jülich GmbH, 52425 Jülich, Germany*

Thomas Bornhake − *Institute of Energy and Climate Research (IEK-13)—Theory and Computation of Energy Materials, Forschungszentrum Jülich GmbH, 52425 Jülich, Germany; Jülich Aachen Research Alliance JARA Energy & Center for Simulation and Data Science (CSD), 52425 Jülich, Germany*

Dirk Bosbach − *Institute of Energy and Climate Research (IEK-6)—Nuclear Waste Management, Forschungszentrum Jülich GmbH, 52425 Jülich, Germany*

Felix Brandt − *Institute of Energy and Climate Research (IEK-6)—Nuclear Waste Management, Forschungszentrum Jülich GmbH, 52425 Jülich, Germany*

Complete contact information is available at: https://pubs.acs.org/10.1021/acs.cgd.3c00809

Notes

The authors declare no competing financial interest.

■ ACKNOWLEDGMENTS

The research leading to these results has received funding from the German Federal Ministry of Education and Research (BMBF) KRIMI project (project number 02NUK056B). The authors gratefully acknowledge the computing time granted by the JARA Vergabegremium and provided on the JARA Partition part of the supercomputers JURECA at Forschungszentrum Jülich and CLAIX at RWTH Aachen University (Project cjiek61).

■ REFERENCES

(1) Brandt, F.; Klinkenberg, M.; Poonoosamy, J.; Bosbach, D. Recrystallization and Uptake of ^{226}Ra into Ba-Rich $(Ba,Sr)SO_4$ Solid Solutions. *Minerals* **2020**, *10*, 812.

(2) Klinkenberg, M.; Weber, J.; Barthel, J.; Vinograd, V.; Poonoosamy, J.; Kruth, M.; Bosbach, D.; Brandt, F. The solid solution-aqueous solution system (Sr, Ba, Ra) SO_4 + H_2O: A combined experimental and theoretical study of phase equilibria at Sr-rich compositions. *Chem. Geol.* **2018**, *497*, 1−17.

(3) Tesch, R.; Kowalski, P. M.; Eikerling, M. H. Properties of the Pt (111)/electrolyte electrochemical interface studied with a hybrid DFT-solvation approach. *J. Phys.: Condens. Matter* **2021**, *33*, 444004.

(4) Rutherford, P.; Dudas, M.; Arocena, J. Heterogeneous distribution of radionuclides, barium and strontium in phosphogypsum by-product. *Sci. Total Environ.* **1996**, *180*, 201−209.

(5) Martin, A. J.; Crusius, J.; Jay McNee, J.; Yanful, E. K. The mobility of radium-226 and trace metals in pre-oxidized subaqueous uranium mill tailings. *Appl. Geochem.* **2003**, *18*, 1095−1110.

(6) Ceccarello, S.; Black, S.; Read, D.; Hodson, M. E. Industrial radioactive Barite scale: suppression of radium uptake by introduction of competing ions. *Miner. Eng.* **2004**, *17*, 323−330.

(7) Fisher, R. S. Geologic and geochemical controls on naturally occurring radioactive materials (NORM) in produced water from oil, gas, and geothermal operations. *Environ. Geosci.* **1998**, *5*, 139−150.

(8) Cheong, O.; Eikerling, M. H.; Kowalski, P. M. Water structures on Pb (100) and (111) surface studied with the Interface force field. *Appl. Surf. Sci.* **2022**, *589*, 152838.

(9) Stack, A. G.; Raiteri, P.; Gale, J. D. Accurate rates of the complex mechanisms for growth and dissolution of minerals using a combination of rare-event theories. *J. Am. Chem. Soc.* **2012**, *134*, 11−14.

(10) Yang, P.; Rampal, N.; Weber, J.; Bracco, J. N.; Fenter, P.; Stack, A. G.; Lee, S. S. Synergistic Enhancement of Lead and Selenate Uptake at the Barite (001)-Water Interface. *Environ. Sci. Technol.* **2022**, *56*, 16801−16810.

(11) Broad, A.; Darkins, R.; Duffy, D. M.; Ford, I. J. Calcite Kinks Grow via a Multistep Mechanism. *J. Phys. Chem. C* **2022**, *126*, 15980−15985.

(12) Bjelobrk, Z.; Rajagopalan, A. K.; Mendels, D.; Karmakar, T.; Parrinello, M.; Mazzotti, M. Solubility of organic salts in solvent-antisolvent mixtures: A combined experimental and molecular dynamics simulations approach. *J. Chem. Theory Comput.* **2022**, *18*, 4952−4959.

(13) Weber, J.; Bracco, J. N.; Yuan, K.; Starchenko, V.; Stack, A. G. Studies of Mineral Nucleation and Growth Across Multiple Scales: Review of the Current State of Research Using the Example of Barite ($BaSO_4$). *ACS Earth Space Chem.* **2021**, *5*, 3338−3361.

(14) Heberling, F.; Vinograd, V. L.; Polly, R.; Gale, J. D.; Heck, S.; Rothe, J.; Bosbach, D.; Geckeis, H.; Winkler, B. A thermodynamic adsorption/entrapment model for selenium (IV) coprecipitation with calcite. *Geochim. Cosmochim. Acta* **2014**, *134*, 16−38.

(15) Poonoosamy, J.; Haber-Pohlmeier, S.; Deng, H.; Deissmann, G.; Klinkenberg, M.; Gizatullin, B.; Stapf, S.; Brandt, F.; Bosbach, D.; Pohlmeier, A. Combination of MRI and SEM to assess changes in the chemical properties and permeability of porous media due to Barite precipitation. *Minerals* **2020**, *10*, 226.

(16) Klinkenberg, M.; Brandt, F.; Baeyens, B.; Bosbach, D.; Fernandes, M. M. Adsorption of barium and radium on montmorillonite: A comparative experimental and modelling study. *Appl. Geochem.* **2021**, *135*, 105117.

(17) Allan, N. L.; Rohl, A. L.; Gay, D. H.; Catlow, C. R. A.; Davey, R. J.; Mackrodt, W. C. Calculated bulk and surface properties of sulfates. *Faraday Discuss.* **1993**, *95*, 273−280.

(18) Pina, C. M.; Becker, U.; Risthaus, P.; Bosbach, D.; Putnis, A. Molecular-scale mechanisms of crystal growth in Barite. *Nature* **1998**, *395*, 483−486.

(19) Jang, Y. H.; Chang, X. Y.; Blanco, M.; Hwang, S.; Tang, Y.; Shuler, P.; Goddard, W. A. The MSXX force field for the barium sulfate-water interface. *J. Phys. Chem. B* **2002**, *106*, 9951−9966.

(20) Bittarello, E.; Bruno, M.; Aquilano, D. Ab initio calculations of the main crystal surfaces of baryte (BaSO4). *Cryst. Growth Des.* **2018**, *18*, 4084−4094.

(21) Bosbach, D. In *Water-Rock Interactions, Ore Deposits, and Environmental Geochemistry: A Tribute to David A. Crerar*; Wood, S. A., Hellmann, R., Eds.; The Geochemical Society, 2002; pp 97−110.

(22) Higgins, S. R.; Bosbach, D.; Eggleston, C. M.; Knauss, K. G. Kink dynamics and step growth on barium sulfate (001): a

hydrothermal scanning probe microscopy study. *J. Phys. Chem. B* **2000**, *104*, 6978−6982.
(23) Pina, C. M.; Jordan, G. Reactivity of mineral surfaces at nanoscale: kinetics and mechanisms of growth and dissolution. In *Nanoscopic Approaches in Earth and Planetary Sciences*; Mineralogical Society of Great Britain: Ireland, 2010; pp 239−323.
(24) de Antonio Gomez, S.; Pina, C. M.; Martin-Bragado, I. Lattice kinetic modeling of the anisotropic growth of two-dimensional islands on Barite (001) surface. *Cryst. Growth Des.* **2013**, *13*, 2840−2845.
(25) Bracco, J. N.; Gooijer, Y.; Higgins, S. R. Hydrothermal atomic force microscopy observations of Barite step growth rates as a function of the aqueous barium-to-sulfate ratio. *Geochim. Cosmochim. Acta* **2016**, *183*, 1−13.
(26) Vital, M.; Daval, D.; Morvan, G.; Martinez, D. E.; Heap, M. J. Barite growth rates as a function of crystallographic orientation, temperature, and solution saturation state. *Cryst. Growth Des.* **2020**, *20*, 3663−3672.
(27) Stack, A. G. Molecular Dynamics Simulations of Solvation and Kink Site Formation at the {001} Barite−Water Interface. *J. Phys. Chem. C* **2009**, *113*, 2104−2110.
(28) Kowacz, M.; Putnis, C.; Putnis, A. The effect of cation: anion ratio in solution on the mechanism of Barite growth at constant supersaturation: Role of the desolvation process on the growth kinetics. *Geochim. Cosmochim. Acta* **2007**, *71*, 5168−5179.
(29) Momma, K.; Izumi, F. VESTA 3 for three-dimensional visualization of crystal, volumetric and morphology data. *J. Appl. Crystallogr.* **2011**, *44*, 1272−1276.
(30) Kurganskaya, I.; Rohlfs, R. D. Atomistic to meso-scale modeling of mineral dissolution: Methods, challenges and prospects. *Am. J. Sci.* **2020**, *320*, 1−26.
(31) Kurganskaya, I.; Trofimov, N.; Luttge, A. A Kinetic Monte Carlo Approach to Model Barite Dissolution: The Role of Reactive Site Geometry. *Minerals* **2022**, *12*, 639.
(32) Abujas-Pereira, J.; Martin-Bragado, I.; Pina, C. M.; Pizarro, J.; Galindo, P. L. A distributed-memory parallel lattice Kinetic Monte Carlo algorithm for crystal growth applied to Barite (001) face. *Cryst. Res. Technol.* **2016**, *51*, 575−585.
(33) Sholl, D. S.; Steckel, J. A. *Density Functional Theory: A Practical Introduction*; John Wiley Sons, 2022.
(34) Andreussi, O.; Dabo, I.; Marzari, N. Revised self-consistent continuum solvation in electronic-structure calculations. *J. Chem. Phys.* **2012**, *136*, 064102.
(35) Fisicaro, G.; Genovese, L.; Andreussi, O.; Mandal, S.; Nair, N. N.; Marzari, N.; Goedecker, S. Soft-Sphere Continuum Solvation in Electronic-Structure Calculations. *J. Chem. Theory Comput.* **2017**, *13*, 3829−3845.
(36) Giannozzi, P.; Baroni, S.; Bonini, N.; Calandra, M.; Car, R.; Cavazzoni, C.; Ceresoli, D.; Chiarotti, G. L.; Cococcioni, M.; Dabo, I.; et al. QUANTUM ESPRESSO: a modular and open-source software project for quantum simulations of materials. *J. Phys.: Condens. Matter* **2009**, *21*, 395502.
(37) Giannozzi, P.; Andreussi, O.; Brumme, T.; Bunau, O.; Buongiorno Nardelli, M.; Calandra, M.; Car, R.; Cavazzoni, C.; Ceresoli, D.; Cococcioni, M.; et al. Advanced capabilities for materials modelling with Quantum ESPRESSO. *J. Phys.: Condens. Matter* **2017**, *29*, 465901.
(38) Perdew, J. P.; Burke, K.; Ernzerhof, M. Generalized gradient approximation made simple. *Phys. Rev. Lett.* **1996**, *77*, 3865−3868.
(39) Vanderbilt, D. Soft self-consistent pseudopotentials in a generalized eigenvalue formalism. *Phys. Rev. B: Condens. Matter Mater. Phys.* **1990**, *41*, 7892−7895.
(40) Andreussi, O.; Hormann, N. G.; Nattino, F.; Fisicaro, G.; Goedecker, S.; Marzari, N. Solvent-aware interfaces in continuum solvation. *J. Chem. Theory Comput.* **2019**, *15*, 1996−2009.
(41) Ringe, S.; Hörmann, N. G.; Oberhofer, H.; Reuter, K. Implicit Solvation Methods for Catalysis at Electrified Interfaces. *Chem. Rev.* **2021**, *122*, 10777−10820.
(42) Schwarz, K.; Sundararaman, R. The electrochemical interface in first-principles calculations. *Surf. Sci. Rep.* **2020**, *75*, 100492.
(43) Rappe, A. K.; Casewit, C. J.; Colwell, K. S.; Goddard, W. A.; Skiff, W. M. UFF, a full periodic table force field for molecular mechanics and molecular dynamics simulations. *J. Am. Chem. Soc.* **1992**, *114*, 10024−10035.
(44) Sheppard, D.; Xiao, P.; Chemelewski, W.; Johnson, D. D.; Henkelman, G. A generalized solid-state nudged elastic band method. *J. Chem. Phys.* **2012**, *136*, 074103.
(45) Henkelman, G.; Uberuaga, B. P.; Jónsson, H. A climbing image nudged elastic band method for finding saddle points and minimum energy paths. *J. Chem. Phys.* **2000**, *113*, 9901−9904.
(46) Jónsson, H.; Mills, G.; Jacobsen, K. W. *Classical and Quantum Dynamics in Condensed Phase Simulations*; World Scientific, 1998; pp 385−404.
(47) Rudin, S.; Kowalski, P.; Klinkenberg, M.; Bornhake, T.; Bosbach, D.; Brandt, F. *Simulation Data for: Simulation of Crystal Growth by an Innovative Hybrid DFT-Continuum Solvation Approach: Kink-Site Formation on Barite (001)*; Jülich DATA, 2023.
(48) Sun, W.; Ceder, G. Efficient creation and convergence of surface slabs. *Surf. Sci.* **2013**, *617*, 53−59.
(49) Tesch, R.; Kowalski, P. M. Hubbard U parameters for transition metals from first principles. *Phys. Rev. B* **2022**, *105*, 195153.
(50) Chibowski, E.; Hołysz, L. Influence of tetradecylamine chloride on the surface freeenergy components and flotability of Barite. *J. Mater. Sci.* **1992**, *27*, 5221−5228.
(51) Stack, A. G.; Rustad, J. R. Structure and Dynamics of Water on Aqueous Barium Ion and the {001} Barite Surface. *J. Phys. Chem. C* **2007**, *111*, 16387−16391.
(52) Persson, I.; Sandström, M.; Yokoyama, H. Structure of the solvated strontium and barium ions in aqueous, dimethyl sulfoxide and pyridine solution, and crystal structure of strontium and barium hydroxide octahydrate. *Z. Naturforschung A* **1995**, *50*, 21−37.
(53) Richens, D. T. *The Chemistry of Aqua Ions: Synthesis, Structure, and Reactivity: A Tour through the Periodic Table of the Elements*; Wiley New York, 1997.
(54) Marcus, Y. Thermodynamics of solvation of ions. Part 5.—Gibbs free energy of hydration at 298.15 K. *J. Chem. Soc., Faraday Trans.* **1991**, *87*, 2995−2999.
(55) Smith, D. W. Ionic hydration enthalpies. *J. Chem. Educ.* **1977**, *54*, 540.
(56) Fenter, P.; McBride, M.; Srajer, G.; Sturchio, N.; Bosbach, D. Structure of Barite (001)- and (210)-water interfaces. *J. Phys. Chem. B* **2001**, *105*, 8112−8119.
(57) Bracco, J. N.; Lee, S. S.; Stubbs, J. E.; Eng, P. J.; Heberling, F.; Fenter, P.; Stack, A. G. Hydration structure of the Barite (001)-water interface: Comparison of x-ray reflectivity with molecular dynamics simulations. *J. Phys. Chem. C* **2017**, *121*, 12236−12248.
(58) Pina, C. M.; Jordan, G. Reactivity of mineral surfaces at nanoscale: kinetics and mechanisms of growth and dissolution. *Nanoscopic Approaches in Earth and Planetary Sciences*; Mineralogical Society of Great Britain: Ireland, 2010; pp 239−323.
(59) Pina, C. M.; Bosbach, D.; Prieto, M.; Putnis, A. Microtopography of the Barite (0 0 1) face during growth:: AFM observations and PBC theory. *J. Cryst. Growth* **1998**, *187*, 119−125.
(60) Wolthers, M.; Nehrke, G.; Gustafsson, J. P.; Van Cappellen, P. Calcite growth kinetics: Modeling the effect of solution stoichiometry. *Geochim. Cosmochim. Acta* **2012**, *77*, 121−134.
(61) Plomp, M.; McPherson, A.; Malkin, A. J. Crystal growth of macromolecular crystals: correlation between crystal symmetry and growth mechanisms. *J. Cryst. Growth* **2002**, *237−239*, 306−311.

https://doi.org/10.1021/acs.cgd.3c00809
Cryst. Growth Des. 2024, 24, 159−170